Computer simulation studies of the soliton model: 3. Non-continuum regimes and soliton interactions

Karna J. Wahlstrand*
Polymers Division, National Bureau of Standards, Gaithersburg, MD 20899, USA
(Received 20 May 1987; accepted 28 July 1987)

We continue the study of the sine–Gordon soliton model, performing stochastic molecular dynamics computer simulations for a wide range of both temperatures and coupling constants. We find three general regimes of behaviour: the continuum limit or non-interacting regime; the pinned or transition-state-theory (TST) limit, where soliton–phonon interactions are important; and the general non-continuum regime, where soliton–soliton interactions of 'multiple soliton effects' are important. In the non-continuum regime, the correlation function changes as a function of temperature and coupling constant. We expect that this will lead to deviations from the continuum limit temperature scaling and soliton energy scaling observed in the dynamics of sine–Gordon systems.

(Keywords: sine–Gordon soliton model; computer simulation; transition state theory; continuous limits; dielectric relaxation; polyethylene)

INTRODUCTION

Recently we studied the sine–Gordon soliton as a model for dielectric relaxation in polyethylene and similar polymers[1-4]. In this model the soliton consists of a freely propagating 180° twist of the chain axis (with a stretch of half a lattice unit). In the presence of an alternating electric field, the soliton moves up and down the chain in Brownian motion, rotating dilute perpendicular dipoles in the process.

Initially we concentrated primarily on continuum limit simulations of the chain at constant temperature[1] and the continuum limit theoretical treatment[1,3,4] (in ref. 1). We investigated the time derivative of the dielectric decay function $C(t)$ (the dipole–dipole correlation function in the case of dilute dipoles) and found diffusive behaviour with characteristic power law of exponent $-1/2$. The simulations were in excellent agreement with the theory at large coupling constants ($(C/A)^{1/2} > 2.9$) and moderate temperature ($T_R = 3.06$).

As the coupling constant was decreased we found increasing deviation from this result[2], and several models were examined as potential explanations. The hopping diffusion model of the soliton[1] gave continuum limit results, and a model of the soliton as a 'relativistic' (with respect to the speed of sound in the crystal) particle moving in an effective periodic potential of the lattice (in ref. 2) gave qualitatively similar results. Both these models assumed that the solitons were non-interacting, so it was concluded[2] that soliton interactions with other solitons ('multiple soliton effects') must be responsible.

In this paper we extend the original[1] sine–Gordon soliton simulations to lower coupling constants and different temperatures to investigate this non-continuum behaviour. In the next section, we review the soliton model and simulation technique. Then we discuss the non-continuum results as a function of temperature and coupling constant. Finally we summarize and give conclusions. In the following paper we apply these results to the temperature dependence of the crystalline (α) dielectric relaxation in polyethylene.

SOLITON MODEL AND SIMULATION

Skinner and Wolynes[3,4] first considered the sine–Gordon soliton model for this problem, which is described by the Hamiltonian:

$$H = \sum_i [A(1-\cos 2\theta_i) + \tfrac{1}{2}C(\theta_i - \theta_{i+1})^2 + \tfrac{1}{2}I\dot{\theta}_i^2] \quad (1)$$

as a one-dimensional problem in θ_i, the angle of rotation of the chain axis from zero at the ith site (two CH_2 units comprising a site). Here A is the magnitude of the (intermolecular) crystal-field potential, and C is the magnitude of the (intramolecular) Hooke's law potential. A represents the correction into crystal register of the half-a-lattice-unit stretch, and C represents effective bond-length and valence-angle distortions. The quantity $(C/A)^{1/2}$ is the characteristic coupling constant of the problem.

If the soliton is viewed as a particle (neglecting its length), we can compute the time correlation function as the product of two step functions (the two-state approximation):

$$C(t) = \langle [2H(\theta_k(0)) - 1][2H(\theta_k(t)) - 1] \rangle \quad (2)$$

where $k = (N+1)/2$ is the centre site on a chain of N sites, and H is the step function:

$$H(\theta) = \begin{cases} 0 & -\pi/2 \leqslant \theta < \pi/2 \\ 1 & \pi/2 \leqslant \theta \leqslant 3\pi/2 \end{cases} \quad (3)$$

which essentially counts soliton passes. Then the derivative of the correlation function can be written as

* Present address: Mission Research Corporation, 5503 Cherokee Avenue, Alexandria, VA 22312, USA

0032-3861/88/020256-07$03.00

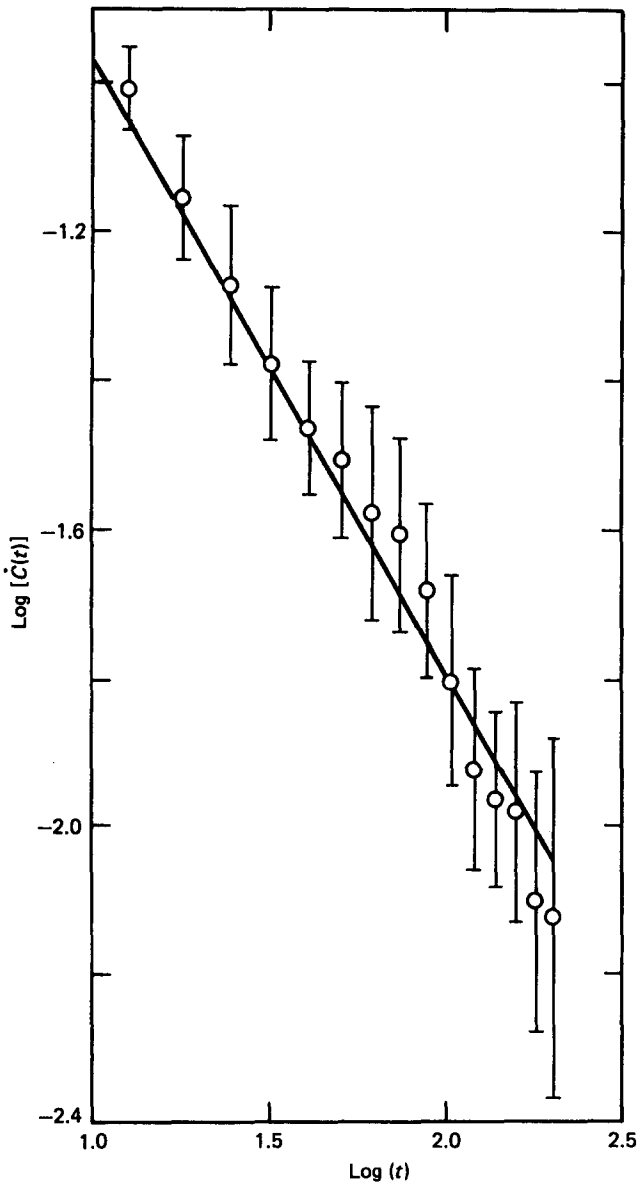

Figure 1 Typical plot of $\log[\dot{C}(t)]$ vs. $\log t$ (for $C/A)^{1/2}=0.8$, $T_R=2.0$ simulation results, $t>1$). The slope is $\bar{\beta}-1$, where the power-law exponent $\bar{\beta}=0.172$

(omitting the factor of 4):

$$\dot{C}(t)=\langle\dot{\theta}_k(0)\delta(\pi/2-\theta_k(0))H(\theta_k(t))\rangle \quad (4)$$

Notice the delta function at the initial position, which allows us to start the simulation in a one-soliton transition state, a chain equilibrated with the centre site k fixed at $\pi/2$, and the sites at $i<k$ near 0 and the sites at $i>k$ near π. It is this rapidly varying correlation-function derivative that is measured by the simulation.

The simulation[1] is a stochastic molecular dynamics simulation of one chain, the neighbouring chains being represented by the crystal-field potential. As in conventional molecular dynamics, the equations of motion are integrated, via the Verlet algorithm[5]. The stochastic part involves the BGK collision model[6]. The collisions are chosen from a Poisson distribution of collision times:

$$P(t)=e^{-\alpha t} \quad (5)$$

where α is the BGK collision frequency $(1/\tau_c)$, which increases as the square root of the temperature. The angular velocity at each site is randomized after each collision by selection from a Boltzmann distribution. We used reduced units of A for energy and temperature (k_BT), I for moment of inertia, and $\omega_0=(A/I)^{1/2}$ for time and frequency. The results are the average of 10000 trajectories. (Further details of the simulation method can be found in ref. 1.)

Forty simulations were done (out to $t=10$) at different coupling constants and temperatures. (A typical simulation took about an hour of CPU time on a Cyber 205 supercomputer.) Power-law behaviour of the correlation-function derivative was found at long times in all but a few cases (where the correlation function was essentially constant), so log–log plots of the correlation-function derivative vs. time were linear (see *Figure 1*). A least-squares fit of the slope $(\bar{\beta}-1)$ yielded a power-law exponent $\bar{\beta}\neq 0.5$ outside the continuum limit regime, and $\bar{\beta}$ varied as a function of temperature and coupling constant. (Only $t>1$ points were fitted.) In addition, best non-linear least-squares fits of the continuum limit correlation-function derivative[1] (normalized, with a one-soliton initial condition):

$$\dot{C}(t)=\frac{1}{\sqrt{2}}\frac{1-e^{-\gamma t}}{(\gamma t-1+e^{-\gamma t})^{1/2}} \quad (6)$$

to the simulation as a function of γ were also done, even outside the continuum limit where the fit was not good, defining γ as a general measure of damping. Strictly speaking, γ is only well defined as a fitted parameter in the continuum limit where (6) holds and where it is defined as the (effective) phenomenological friction constant for soliton motion (the damping constant divided by the effective soliton mass in the Fokker–Planck derivation). However, as a crude measure it turns out to be quite useful quantitatively as well as qualitatively in discussing the general non-continuum behaviour as well (see below).

NON-CONTINUUM BEHAVIOUR

General features

In general, the sine–Gordon model correlation-function derivative showed three regimes of behaviour. Continuum limit behaviour, where (6) was fitted within the error bounds discussed in ref. 1, and a constant power-law exponent of $\bar{\beta}=0.5$ independent of both coupling constant and temperature was found, held for all temperatures and coupling constants $(C/A)^{1/2}\gtrsim 1$ such that $\beta E_K\gtrsim 4$, where E_K is defined as the continuum limit soliton energy $4(C/A)^{1/2}$ ($\beta\equiv 1/k_BT$) for the purposes of delineating regimes (see below)). (In other words, $(C/A)^{1/2}\gtrsim T_R$ in the continuum limit cases.) Notice that temperature as well as coupling constant determines continuum limit behaviour (see *Table 1*). This is probably because, in agreement with our theoretical studies[1-3], soliton interactions determine the regimes, and they are a function of βE_K through the soliton density. When $(C/A)^{1/2}\lesssim 1$ and $\beta E_K\gtrsim 4$, the correlation-function derivatives showed a constant plateau value at long times (see *Figure 2* and *Table 2*), which we shall discuss below as transition-state-theory (TST) or pinned limit behaviour, demonstrating discreteness effects as discussed in ref. 2.

Table 1 Results of nine continuum limit simulation cases

$(C/A)^{1/2}$	T_R	βE_K	$\bar{\beta}^a$	γ
1.0	0.4	10.0	0.663	0.50
1.0	1.0	4.0	0.472	1.00
2.0	0.2	40.0	0.624	0.97
2.0	0.4	20.0	0.509	1.73
2.0	0.8	10.0	0.437	2.63
2.0	1.0	8.0	0.538	2.85
2.0	1.6	5.0	0.570	3.07
2.0	2.0	4.0	0.493	4.62
10.0	8.0	5.0	0.633	35.4

[a] Theoretical value $\bar{\beta}=0.5$

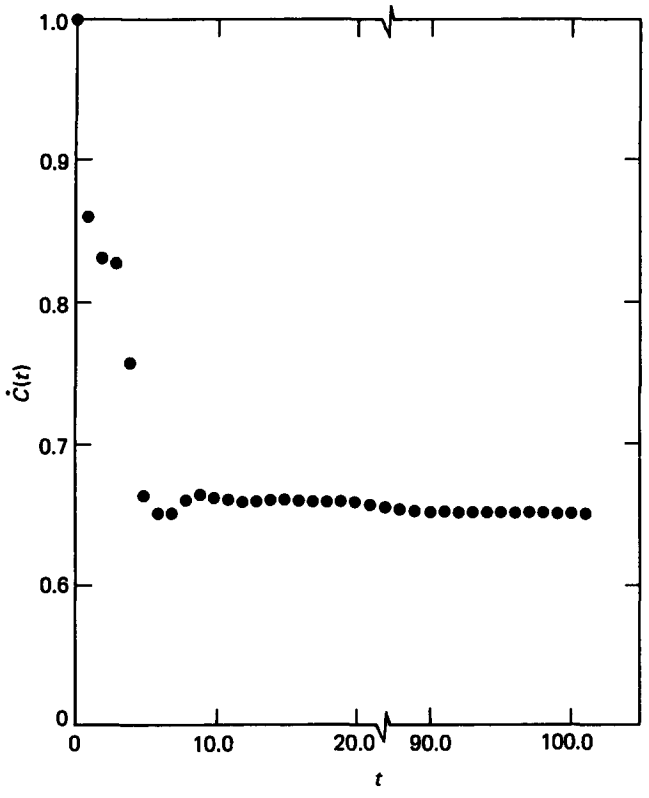

Figure 2 Typical transition-state-theory case behaviour, for $(C/A)^{1/2}=0.5$ and $T_R=0.2$, shown out to $t=100$ in a special long simulation

These two regimes show essentially non-interacting solitons.

In the remaining general non-continuum regime ($\beta E_K \lesssim 4$), soliton interactions are important and the power-law exponent is a function of both coupling constant (through interactions of solitons with phonons) and temperature (through interactions of solitons with other solitons). The results of these simulations are shown in *Table 3* and are discussed in detail below. The range of exponents observed here was roughly $-0.5<\bar{\beta}<1.0$ at the temperatures we investigated. (Good higher-temperature data, which would produce lower $\bar{\beta}$ values, were difficult to obtain because of noise in those simulations. An indication of the typical error bars on $\bar{\beta}$ can be obtained by comparing the values in *Table 1* with the theoretical value $\bar{\beta}=0.5$. Typical γ value error bars are also a continuum limit phenomenon, as in ref. 1.)

In addition, soliton length was observed and discrete soliton energy was calculated. Soliton length is independent of temperature in the continuum limit, but decreases with increasing temperature in the non-continuum regime. As expected, transition-state-theory cases have unit soliton lengths ($(C/A)^{1/2}\lesssim 1$). Discrete soliton energy E_K^{dis} was calculated as the difference between the (equilibrated) one-soliton transition-state and ground-state mean energies as in ref. 1, and is shown in *Figure 3*. For values of $(C/A)^{1/2}\gtrsim 2$, E_K^{dis} approached the limiting behaviour (in reduced units):

$$E_K^{dis} \approx 3.76(C/A)^{1/2} - 3.04 \quad (7)$$

(linear in $(C/A)^{1/2}$). As expected, as $(C/A)^{1/2}\to 0$, $E_K^{dis}\to 1$ and the discrete soliton energy becomes the same as the barrier height A in the independent-wells (low-coupling) limit. We shall now discuss non-continuum (followed by transition-state-theory) behaviour in more detail.

Temperature dependence

It was found that the power-law exponent $\bar{\beta}$ decreases with increasing temperature linearly in the log of temperature for all coupling constants in the non-continuum regime according to:

$$\bar{\beta} = (-0.31 \pm 0.05)\ln(T_R/T_\beta) \quad (8)$$

where T_β is a function of the coupling constant $(C/A)^{1/2}$ and is plotted below in *Figure 8a*. A master plot of $\bar{\beta}$ vs. log temperature for three coupling-constant values is

Table 2 Results of seven transition-state-theory simulation cases

$(C/A)^{1/2}$	T_R	βE_K	Plateau values	γ
0.20	0.2	4.0	0.723 ± 0.007	0.15
0.25	0.2	5.0	0.693 ± 0.008	0.18
0.50	0.1	20.0	0.688 ± 0.006	0.17
0.50	0.2	10.0	0.655 ± 0.003^a	0.19
0.50	0.4	5.0	0.604 ± 0.005	0.28
1.0	0.2	20.0	0.631 ± 0.006	0.25

[a] A plateau value from $t=100$ version (more accurate); 0.688 was obtained in $t=10$ version, and used in plot in *Figure 9* for consistency with other points

Table 3 Results of 24 general non-continuum simulation cases

$(C/A)^{1/2}$	T_R	βE_K	$\bar{\beta}$	γ
0.0001	2.00	0.002	0.629	0.74
0.001	4.00	0.001	0.413	1.57
0.10	2.00	0.20	0.606	0.74
0.20	2.00	0.40	0.562	0.80
0.33	2.00	0.67	0.457	0.93
0.50	0.60	3.33	0.765	0.34
0.50	0.80	2.50	0.640	0.56
0.50	1.00	2.00	0.619	0.55
0.50	1.25	1.60	0.552	0.68
0.50	1.50	1.33	0.390	0.92
0.50	2.00	1.00	0.327	1.15
0.67	2.00	1.33	0.199	1.49
0.80	2.00	1.60	0.172	1.70
1.00	2.00	2.00	0.213	2.10
1.00	3.06	1.31	−0.016	3.27
1.00	8.00	0.50	−0.177	7.50
1.25	2.00	2.50	0.178	2.95
1.50	2.00	3.00	0.305	3.48
1.75	2.00	3.50	0.394	4.04
2.00	3.06	2.61	0.337	6.50
2.00	4.00	2.00	0.326	8.80
2.00	10.0	0.80	0.076	19.2
2.00	40.0	0.20	−0.306	68.2
10.0	20.0	2.00	−0.063	462

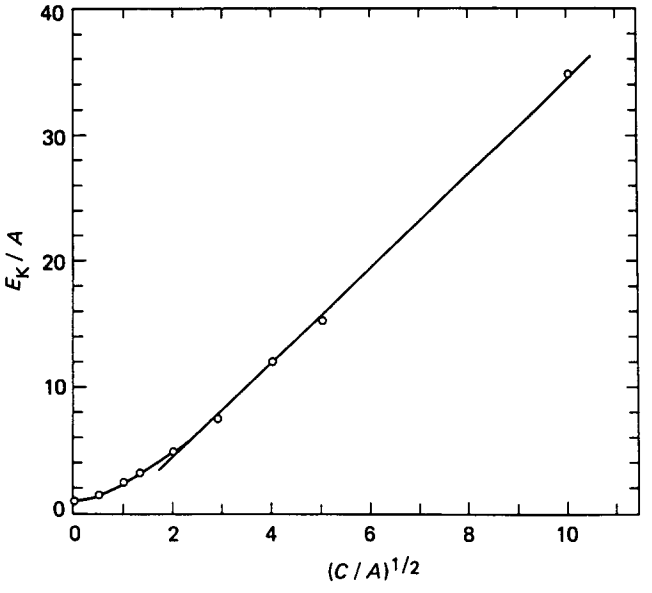

Figure 3 Discrete soliton energy E_K^{dis} as a function of coupling constant $(C/A)^{1/2}$

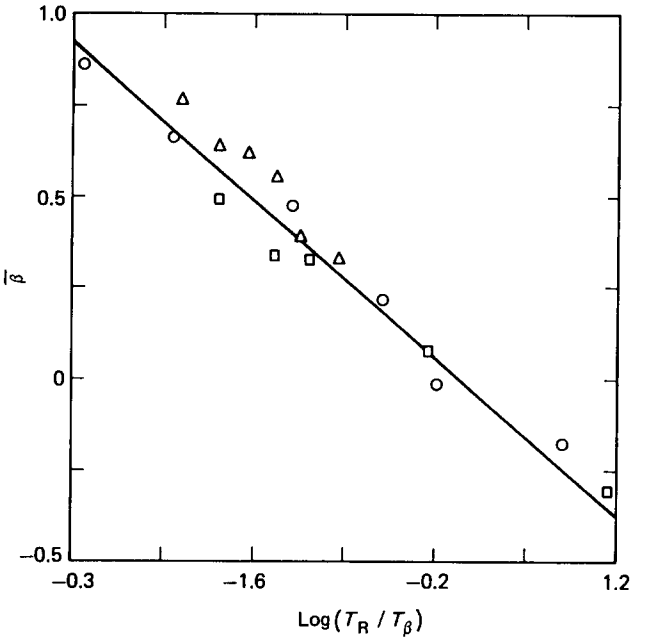

Figure 4 Master plot of power-law exponent $\bar{\beta}$ vs. $\log(T_R/T_\beta)$ for non-continuum regime simulations with $(C/A)^{1/2} = 0.5$ (△), 1.0 (○) and 2.0 (□). The slope is -0.31 ± 0.05

shown in *Figure 4*. This means that the time correlation function changes with temperature in the non-continuum regime, and is a result of soliton–soliton interactions.

Continuum solitons do not change shape or speed upon collision with other solitons. But non-continuum solitons interact, in that two solitons repel each other, a soliton and an antisoliton (a soliton with asymptotic positions reversed) attract and then annihilate and re-create each other, and phonons may create soliton pairs[7–9]. We observed in ref. 2 than an increasing barrier height causes the correlation-function derivative to drop off less rapidly. Thus the decrease in the power-law exponent $\bar{\beta}$ and the increase in soliton density with increasing temperature could be interpreted as other solitons acting as 'effective barriers' to soliton propagation.

A master plot of the log of the damping constant γ vs. the log of the temperature for three coupling-constant values is shown in *Figure 5*. In all regimes (not restricted to non-continuum cases) the behaviour is linear according to the equation:

$$\ln \gamma = (0.91 \pm 0.10) \ln(T_R/T_\gamma) \tag{9}$$

where T_γ is a function of the coupling constant $(C/A)^{1/2}$ and is plotted below in *Figure 8b* for the non-continuum regime. This means that the damping constant increases with increasing temperature according to the power law:

$$\gamma \approx T_R^{0.91 \pm 0.10} \tag{10}$$

(Errors bars in γ are quite large[1] in the continuum regime, but decrease with coupling constant.)

A weak power-law dependence of the damping constant on temperature is also predicted through the Einstein relation $D = 1/\beta m^* \gamma$ (where m^* is the effective soliton mass) for the diffusion constant D for continuum limit double-well soliton theories in the literature. Specifically, Wada and Ishiuchi[10] derive $D \sim T^2$ for sine–Gordon solitons; Wada and Schrieffer[11] derive $D \sim T^2$ for ϕ^4 solitons, giving $\gamma \sim T^{-1}$ (decreasing weakly with increasing temperature); and Sahni and Mazenko[12] derive $D \sim T^{1/2}$ for sine–Gordon solitons, giving $\gamma \sim T^{1/2}$, increasing weakly with increasing temperature. The latter behaviour is most similar to our result, probably because multisoliton configurations were considered in that calculation. Notice that the BGK collision frequency α also increases with the square root of the temperature, and gives a molecular interpretation to at least some of the damping.

Coupling-constant dependence

A plot of the damping constant γ vs. the coupling constant for $T_R = 2.0$ is shown in *Figure 6*. The damping

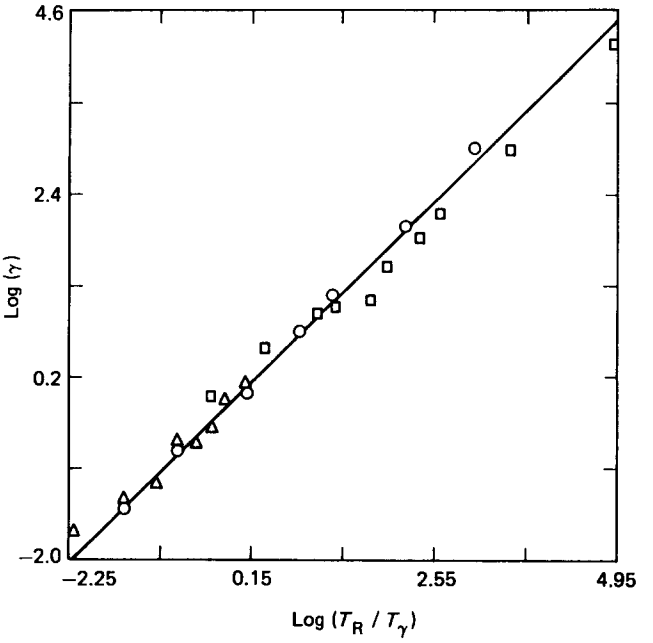

Figure 5 Master plot of log damping constant (log γ) vs. $\log(T_R/T_\gamma)$ for non-continuum regime simulations with coupling constants $(C/A)^{1/2} = 0.5$ (△), 1.0 (○) and 2.0 (□). The slope is 0.91 ± 0.10

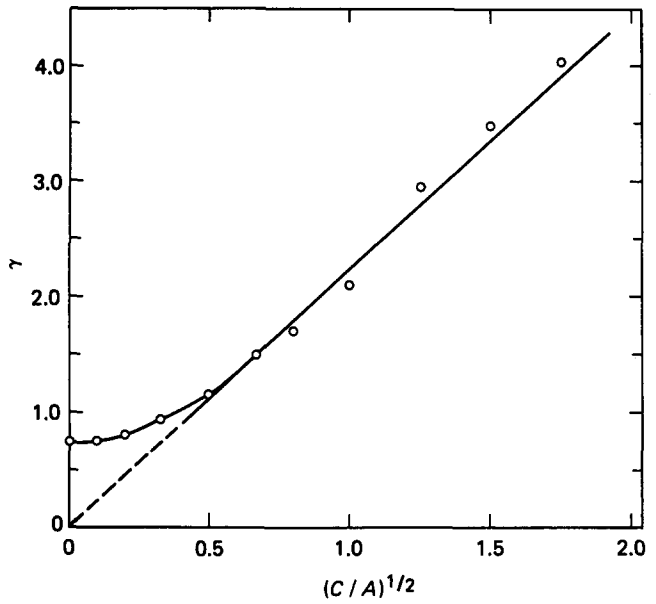

Figure 6 Plot of damping constant γ vs. coupling constant $(C/A)^{1/2}$ for $T_R = 2.0$. The slope at larger coupling-constant values is 2.25

constant increases with coupling constant, linearly with slope 2.25 above $(C/A)^{1/2} \approx 0.5$, and levels off to a constant (which depends on the temperature) as the coupling constant goes to zero. Notice that the behaviour is qualitatively similar to that of the discrete soliton energy vs. coupling constant (see *Figure 3*). This agrees with the fact that the calculation of the diffusion constant for continuum limit sine–Gordon solitons of Wada and Ishiuchi[10] predicts that γ should be proportional to E_K^{dis} in that limit.

The qualitative behaviour of γ with $(C/A)^{1/2}$ is also similar to that of the soliton length vs. coupling constant (see ref. 1 and also above). Soliton length is constant at one unit below $(C/A)^{1/2} \approx 0.5$, and proportional to $(C/A)^{1/2}$ at higher $(C/A)^{1/2}$ values. It makes sense that γ is probably proportional to soliton length because 'phenomenological friction' should depend on the size of a long object being approximated as a particle (finite size effects). If the soliton really were a 'particle' of constant size, this would not be true, and γ might be proportional to the BGK collision frequency α and independent of $(C/A)^{1/2}$.

The behaviour of the power-law exponent $\bar{\beta}$ with coupling constant is interesting because it reflects the competing effects of damping and the effective barriers to soliton propagation caused by discreteness effects in the non-continuum regime, a result of soliton–phonon coupling. This behaviour is shown in *Figure 7* for $T_R = 2.0$. As the coupling constant goes to zero it levels off to a temperature-dependent constant, and at continuum limit values it is constant at 0.5 for all temperatures. In the non-continuum regime in the example at $T_R = 2.0$, for $(C/A)^{1/2}$ between about 0.15 and 0.67, $\bar{\beta}$ decreases linearly with $(C/A)^{1/2}$ with a slope of about -0.40; between 0.67 and 1.25, $\bar{\beta}$ is about constant at 0.20; and between 1.25 and 2.0, $\bar{\beta}$ increases linearly with $(C/A)^{1/2}$ with a slope of about $+0.75$.

This behaviour can be understood from the γ vs. $(C/A)^{1/2}$ behaviour described above and by examining the effective periodic potential magnitude ω_{eff}^2 of discreteness effects determined by Currie *et al.*[7] and shown in our reduced units in ref. 2. Briefly, ω_{eff}^2 is constant at 4.0 for $(C/A)^{1/2} \lesssim 1$, and drops rapidly to zero as the coupling constant increases to about 2.8. It can now be seen that in the region where $\bar{\beta}$ decreases with $(C/A)^{1/2}$, the damping γ is increasing with $(C/A)^{1/2}$ and ω_{eff}^2 is fixed, and since (from ref. 2) increased damping causes a less rapid drop in the correlation-function derivative, the net effect is that of increasing damping causing decreasing $\bar{\beta}$ in this lowest part of the non-continuum regime. At higher values of $(C/A)^{1/2}$ in the non-continuum regime, this effect competes with a decreasing effective discreteness barrier height ω_{eff}^2, which would tend to increase $\bar{\beta}$ (cause a more rapid drop in the correlation-function derivative), and $\bar{\beta}$ remains roughly constant. As $(C/A)^{1/2}$ increases further, this effect dominates the damping, and $\bar{\beta}$ does indeed increase with $(C/A)^{1/2}$ until it reaches the continuum limit value of 0.5.

Thus the lowest part of the $\bar{\beta}$ vs. $(C/A)^{1/2}$ non-continuum regime is dominated by damping, the highest part is dominated by effective barriers ω_{eff}^2 due to discreteness effects, and the region in between involves approximate cancellation of these two competing effects. (From ref. 2 we see that $\bar{\beta}$ would also increase from increasing relativity as $(C/A)^{1/2} \to 0$, but this would not be expected to be a significant effect here, because the thermal root-mean-square reduced velocity v/c_0, where c_0 is the soliton maximum velocity, does not get above 0.55 or 0.60 in most applications.) In this way the $\bar{\beta}$ vs. $(C/A)^{1/2}$ curve reflects phonon–soliton interactions, also a non-continuum phenomenon.

Finally, it should be noticed that the non-continuum regime is completely characterized quantitatively as well as qualitatively by the simulations done here. Combining (8) and (9), we can relate $\bar{\beta}$ and γ at the same temperature as:

$$\bar{\beta} = (-0.34 \pm 0.07) \ln(\gamma R) \qquad (11)$$

where $R = T_\gamma / T_{\bar{\beta}}$ is also a function of $(C/A)^{1/2}$ as shown in *Figure 8c*. Using measured values of $\bar{\beta}$ and γ from the simulations, and equations (8), (9) and (11), $T_{\bar{\beta}}$, T_γ and R as functions of $(C/A)^{1/2}$ are given in *Table 4* and plotted as smooth functions suitable for interpolation in *Figure 8*. Thus $\bar{\beta}$ and γ can be calculated for any non-continuum coupling constant and temperature.

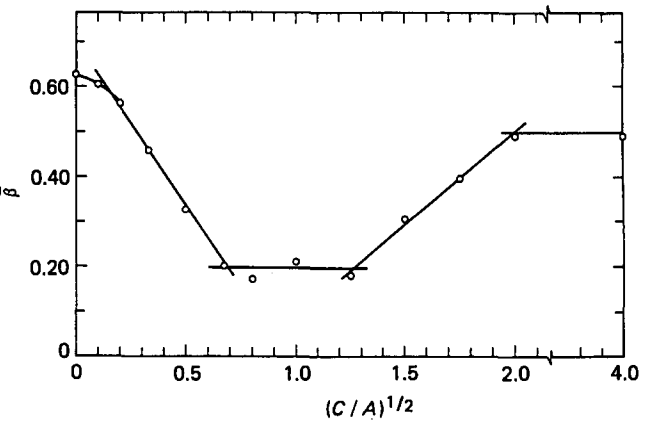

Figure 7 Plot of power-law exponent $\bar{\beta}$ vs. coupling constant $(C/A)^{1/2}$ for $T_R = 2.0$ (see text for slopes)

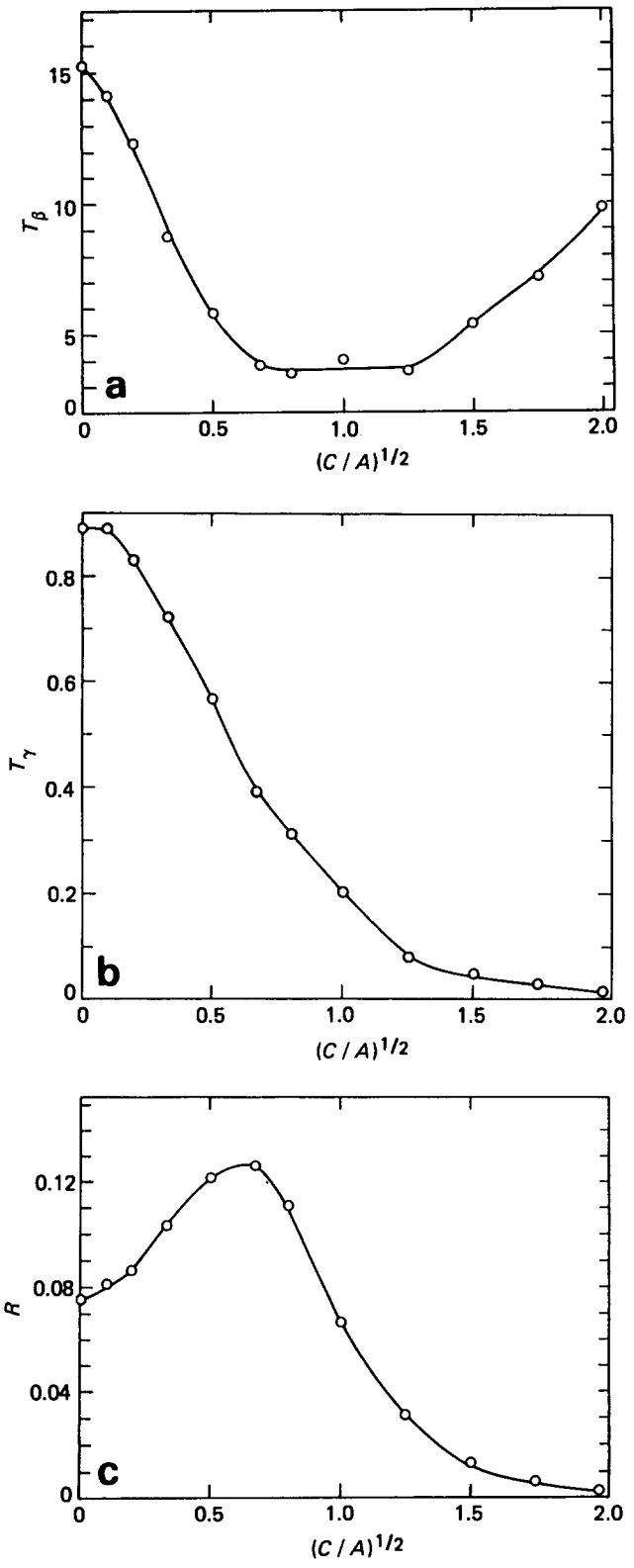

Figure 8 Parameters for the complete quantitative characterization of the non-continuum regime, as a function of coupling constant $(C/A)^{1/2}$: (a) T_β vs. $(C/A)^{1/2}$, (b) T_γ vs. $(C/A)^{1/2}$ and (c) $R = T_\gamma/T_\beta$ vs. $(C/A)^{1/2}$

Pinned/TST limit

As we noted above, when $\beta E_K \gtrsim 4$ and $(C/A)^{1/2} \lesssim 1$, the correlation-function derivative is constant at long times and we have pinned or transition-state-theory (TST) limit behaviour (see *Figure 2*). $(C/A)^{1/2} \approx 1$ is the borderline coupling-constant value, showing continuum limit behaviour for $T_R = 0.4$ ($\beta E_K = 10.0$) and transition-state-theory behaviour for $T_R = 0.2$ ($\beta E_K = 20.0$).

The trajectories observed for the θ_i at different i illustrate the TST behaviour. For $i < (N+1)/2$, the θ_i start near zero in the left well of the crystal-field potential and stay oscillating around the well bottom. For $i > (N+1)/2$, the θ_i start and stay oscillating near π in the right well bottom. For the centre site $i = (N+1)/2$, θ_i starts at the barrier top and rapidly drops into the left or right well and stays there. This centre site behaviour is what one would expect for an isolated transition-state-theory 'reaction'; such behaviour is not surprisingly the result of a non-interacting soliton with very low coupling ($C \ll A$) between neighbouring θ_i. (The off-diagonal correlation functions, $i \neq j$, are zero in the TST simulation cases.) When $\beta E_K < 4$, however, T_R is too high and the damping (interaction with surrounding polymer chains or the physical environment) is too high for TST behaviour and the usual non-continuum limit behaviour results.

In comparing with transition-state theory, the plateau value is the ratio of the true activated event rate constant k to the transition-state-theory rate constant k_{TST}. k/k_{TST} is plotted as a function of the damping constant γ in *Figure 9*. It shows linear behaviour which fits the formula:

$$k/k_{TST} \approx -0.92\gamma + 0.861 \qquad (12)$$

in the cases we studied. Notice that the decrease in plateau value k/k_{TST} is in qualitative agreement with the (non-linear) results of Skinner and Wolynes[13-15] and Hynes[16] for the case of single barrier crossing.

The non-continuum effect observed in this regime is soliton–phonon coupling, with consequent damping and pinning. Physically, the soliton 'radiates phonons' and decreases in velocity until it is 'pinned' in a particular site (i) well[7]. For this to happen it has to have both a low enough coupling constant for there to be discreteness barriers ω_{eff}^2 to soliton propagation and also a low enough temperature to be below the pinning velocity $\beta_{pin} = v/c_0$. Currie *et al.*[7] estimate:

$$\beta_{pin} \approx (\tfrac{1}{8}\omega_{eff}^2)^{1/2} \qquad (C/A)^{1/2} \lesssim 1 \qquad (13)$$

(in our units). Since here $\omega_{eff}^2 \approx 4$ according to their calculations[7], $\beta_{pin} \approx \frac{1}{2}$. In our units:

$$\beta_{pin} = 1/(\beta E_K)^{1/2} \qquad (14)$$

so $v/c_0 \lesssim \beta_{pin}$ is equivalent to $\beta E_K \gtrsim 4$, which is the

Table 4 Non-continuum parameters T_β, T_γ and R as functions of $(C/A)^{1/2}$ calculated from simulation data

$(C/A)^{1/2}$	T_β	T_γ	R
0.001	15.2	0.887	0.075
0.10	14.1	0.887	0.081
0.20	12.3	0.830	0.086
0.33	8.74	0.720	0.103
0.50	5.74	0.565	0.121
0.67	3.80	0.389	0.126
0.80	3.48	0.309	0.110
1.00	3.98	0.199	0.066
1.25	3.55	0.078	0.031
1.50	5.35	0.044	0.013
1.75	7.13	0.024	0.006
2.00	9.81	0.012	0.002

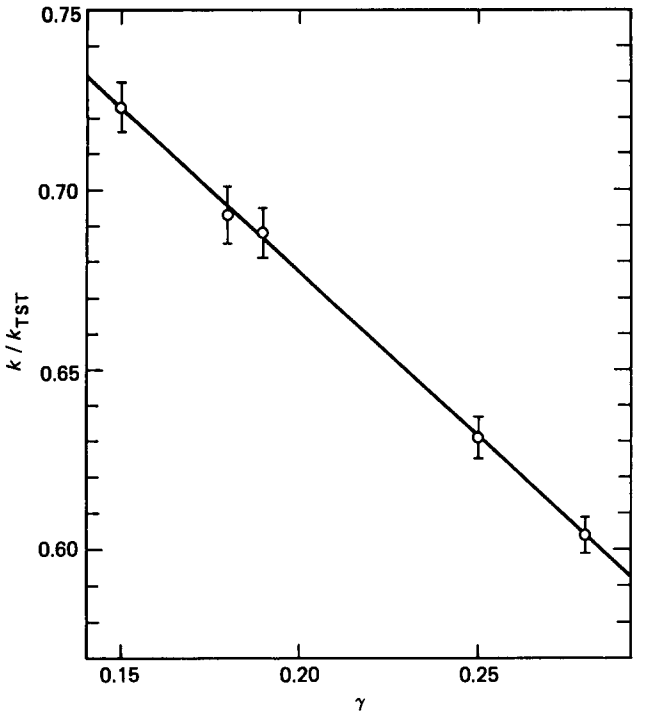

Figure 9 Plateau values k/k_{TST} as a function of damping constant γ in the TST/pinned limit simulation cases ($t = 10$ plateau values are used)

condition we found for TST/pinned limit behaviour. Thus we have quantitative agreement with Currie *et al.* on the region of pinned limit behaviour in sine–Gordon soliton systems.

CONCLUSION

As we have seen, there are basically three regimes of sine–Gordon soliton behaviour, based on the nature and extent of interactions in the system. The non-interacting regime is the continuum limit, characterized by $\beta E_K \gtrsim 4$ and coupling constants greater than 1. Soliton–phonon interactions are important if the coupling constant is $\lesssim 1$, and soliton–soliton interactions are important if $\beta E_K < 4$.

This βE_K cutoff for continuum limit behaviour has been seen in theoretical calculations and verified by experiments on different sine–Gordon soliton-related systems. Takayama and Sato[17] compared transfer integral calculations with numerical results and found that ideal soliton gas phenomenology, which is based on continuum limit and non-interacting soliton approximations, breaks down below about $\beta E_K \lesssim 5$. Nuclear spin–lattice relaxation time studies[18] of the one-dimensional (1D) ferromagnet $CsNiF_3$ show agreement with a continuum limit model for $\beta E_K \gtrsim 2.6$, and similar experiments[19] on the 1D antiferromagnet TMMC show agreement with continuum coherent models in the absence of impurities and continuum incoherent models in the presence of impurities for $\beta E_K \gtrsim 2.5$.

In addition, the experiments on the quasi-1D magnetic systems (the best-characterized sine–Gordon soliton systems to date) demonstrate rather generally that dynamic properties scale with temperature and continuum soliton energy (coupling constant) in the continuum limit. The continuum soliton energy E_K in the 1D antiferromagnet TMMC is proportional to the magnetic field H, and in the 1D ferromagnet $CsNiF_3$ it is proportional to the square root of H. The spin–lattice relaxation time T_1 scales in H and T for $CsNiF_3$ (ref. 18) and for TMMC both with and without impurities[19]. The electron spin resonance linewidths[18] and neutron scattering intensities[20] also scale in H and T for $CsNiF_3$. Below the cutoff of $\beta E_K \approx 2.6$ a plot of $\ln(T/T_1)$ vs. $H^{1/2}/T$ shows deviations from linearity due to non-continuum effects[18] for $CsNiF_3$.

In ref. 1 we predicted that in the continuum limit the one-soliton relaxation time τ_0 scales in temperature:

$$\tau_0^{-1} = \frac{16\eta_0^2}{\beta m^* \pi \gamma^2} \tag{15}$$

(where η_0 is the soliton density, a function of βE_K, and m^* is the effective soliton mass), such that Cole–Cole plots of the frequency-dependent dielectric constant $\varepsilon^*(\omega)$ in polyethylene should be independent of temperature (scale) in the continuum limit. We have seen in this paper that the time correlation function changes with temperature outside the continuum limit. In the following paper we shall show how this applies to experimental dielectric relaxation results for polyethylene.

ACKNOWLEDGEMENT

I acknowledge support from a 1984 National Research Council Postdoctoral Research Associateship.

REFERENCES

1 Wahlstrand, K. J. *J. Chem. Phys.* 1985, **82**, 5247
2 Wahlstrand, K. J. and Wolynes, P. G. *J. Chem. Phys.* 1985, **82**, 5259
3 Skinner, J. L. and Wolynes, P. G. *J. Chem. Phys.* 1980, **73**, 4015
4 Skinner, J. L. and Wolynes, P. G. *J. Chem. Phys.* 1980, **73**, 4022
5 Verlet, L. *Phys. Rev.* 1967, **159**, 98
6 Bohm, D. and Gross, E. P. *Phys. Rev.* 1949, **75**, 1864
7 Currie, J. F., Trullinger, S. E., Bishop, A. R. and Krumhansl, J. A. *Phys. Rev.* (*B*) 1977, **15**, 5567
8 Nakajima, K., Sawada, Y. and Onodera, Y. *Phys. Rev.* (*B*) 1978, **17**, 170
9 Aubry, S. *J. Chem. Phys.* 1976, **64**, 3392
10 Wada, Y. and Ishiuchi, H., *J. Phys. Soc. Japan* 1981, **51**, 1372
11 Wada, Y. and Schrieffer, J. R. *Phys. Rev.* (*B*) 1978, **18**, 3897
12 Sahni, P. S. and Mazenko, G. F. *Phys. Rev.* (*B*) 1979, **20**, 4674
13 Skinner, J. L. and Wolynes, P. G. *J. Chem. Phys.* 1980, **72**, 4913
14 Skinner, J. L. and Wolynes, P. G. *J. Chem. Phys.* 1978, **69**, 2143
15 Skinner, J. L. and Wolynes, P. G. *Physica* (*A*) 1979, **96**, 561
16 Hynes, J. T. *Chem. Phys. Lett.* 1981, **79**, 344
17 Takayama, H. and Sato, G. *J. Phys. Soc. Japan* 1982, **51**, 3120
18 Benner, H., Seitz, H., Wiese, J. and Boucher, J. P. *J. Magn. Magn. Mater.* 1984, **45**, 354
19 Boucher, J. P., Benner, H., Devreux, F., Regnault, L. P., Rossat-Mignod, J., Dupas, C., Renard, J. P., Bouillot, J. and Stirling, W. G. *Phys. Rev. Lett.* 1982, **48**, 431
20 Steiner, M. and Kjems, J. K. in 'Solitons and Condensed Matter Physics', (Eds. A. R. Bishop and T. Schneider), Springer, New York, 1978